boxylate peak location to be greatly influenced by the phasing of the spectrum when the uncoordinated peak moves downfield. In view of the fact that the calculations show very little difference between the EDTA and PDTA peaks over the accessible temperature range, no attempt was made to overcome this problem. The values of ΔH and ΔS for the coordinated $\rightleftharpoons$ uncoordinated equilibria are summarized in Table III. The value of ΔH for EDTA found in this work, −14.2 kJ mol^{-1}, is in reasonable agreement with the previous estimate of −12.2 kJ mol^{-1} (25% uncoordinated).[4]

Examination of Figure 3 indicates that only the equilibrating carboxylate resonance appears to violate the Curie law. One would expect, however, that all resonances would be affected by the equilibration of the carboxylate and, hence, that all the resonances should violate the Curie law. That this is not observed is explained by reference to the *N*-EtED3A spectrum. The spectrum of this 100% pentadentate ligand corresponds quite well to the spectra of the other ligands, indicating that the shift differences between pentadentate and hexadentate forms are very small except for the carboxylates. This is consistent with the fact that contact shifts transmitted through oxygen are much smaller than those transmitted through nitrogen.[18] Thus, the deviations from the Curie law of these resonances are small and, hence, not observable over experimental error.

All attempts to slow the exchange rate so that the coordinated and uncoordinated peaks could be observed directly were unsuccessful. This failure is not surprising since the percentage of 5-coordinate species shifts dramatically in the available low-temperature region toward more pentadentate. A ^{13}C NMR spectrum of Ni(EDTA)$^{2-}$ obtained at 125 MHz did not contain the broad carboxylate peak or new peaks at the "frozen" positions. Assuming that the peak was not observed because of kinetic broadening, the rate constant for the reaction is estimated to be approximately 3×10^5 s^{-1} in reasonable agreement with the water-exchange rate for Ni(H_2O)Y^{2-} of 7×10^5 s^{-1} estimated by ^{17}O NMR.[4]

This work shows that the enthalpy of coordination of the sixth EDTA site is endothermic and very small, and therefore, the position of the equilibrium is easily changed by slight changes in solution conditions, temperature, or structure. The disagreement in the literature can be explained at least in part by this sensitivity.

Acknowledgment. The 125-MHz ^{13}C NMR spectrum was provided by the Southern New England High-Field NMR Facility at Yale University. A Merck Foundation faculty development grant is acknowledged.

(18) Evilia, R. F.; Reilley, C. N. *J. Coord. Chem.* **1973**, *3*, 7–16.

Contribution from the Department of Chemistry, Faculty of Science, Nara Women's University, Nara 630, Japan

Circular Dichroism of Chromium(III) Complexes. 10. Circular Dichroism Spectra in the Spin-Forbidden Transitions of $Cr^{III}(N)_6$ Type Complexes with Chiral Diamines

SUMIO KAIZAKI,* MIEKO ITO, NORIKO NISHIMURA, and YUKIE MATSUSHITA

Received October 18, 1984

Room-temperature solution circular dichroism (CD) spectra were measured in the spin-forbidden ^2E_g, $^2T_{1g} \leftarrow {}^4A_{2g}$ d–d transitions of the diastereomers of $[Cr(en)_x(diamine)_{3-x}]^{3+}$ (x = 0, 2), *cis*-$[Cr(NH_3)_2(diamine)_2]^{3+}$, and $[Cr(NH_3)_4(diamine)]^{3+}$, where the diamines used were (*R*)- or (*S*)-propylenediamine and (1*R*,2*R*)- or (1*S*,2*S*)-1,2-*trans*-cyclohexanediamine. The differences in observed CD spectra between each pair of the diastereomers were accounted for by separability and additivity of the configurational and vicinal CD effects. Consistent assignments for these configurational and vicinal CD peaks to the doublet ← quartet electronic transitions were made in connection with the CD in the spin-allowed $^4T_{2g} \leftarrow {}^4A_{2g}$ transitions on the basis of the theoretical approaches for the energy ordering and the rotational strengths between the spin-forbidden and the spin-allowed transitions; e.g., four vicinal CD peaks in the spin-forbidden transitions of the tris(diamine) complexes were assigned to the $2\bar{A}(^2E_g)$, $\bar{E}(^2E_g)$, $^2A_2(^2T_{1g})$, and $^2E(^2T_{1g})$ from the lower frequency side. This is the first demonstration by the room-temperature solution CD measurements for the ^2E_g split components due to the electronic transitions to the Kramers doublets ($2\bar{A}$ and $\bar{E}$) with a small spacing of less than 100 cm^{-1}.

Introduction

In our previous papers of this series,[1–4] room-temperature solution circular dichroism (CD) spectra in the spin-forbidden ^2E_g, $^2T_{1g} \leftarrow {}^4A_{2g}$ transitions of trigonal and tetragonal Cr(III) complexes have been examined in comparison with those in the first spin-allowed $^4T_{2g} \leftarrow {}^4A_{2g}$ transitions. As a result, it has been demonstrated that weak but sharp well-resolved CD peaks in the spin-forbidden transitions can be elucidated by the close correlation (spin–orbit coupling) between the quartet ($^4T_{2g}$) and doublet (^2E_g and $^2T_{1g}$) excited states. Still, there have remained some ambiguous elucidations of the spin-forbidden transitions even for one of the most popular complexes, $[Cr(en)_3]^{3+}$, though the understanding of chiroptical spectra of this complex in both the spin-forbidden and the first spin-allowed transitions has much advanced in experiments and theories for the last decade.[1,5–14] The low-temperature single-crystal spectroscopic studies[5–8] have confirmed our previous assignments[1] of the lowest frequency CD peak to the spin-forbidden $^2E_g \leftarrow {}^4A_{2g}$ transition and have substantiated the splitting of the ^2E_g state with a spacing of 18 cm^{-1} and the overlapping of the $^2T_{1g}$ split components with the vibronic progression of the ^2E_g origins. However, they are in some disagreement with theoretical treatments.[1,6a,9] Thus, it is important to reexamine whether room-temperature solution CD peaks in this region arise from the electronic or vibronic origins. For this

(1) Kaizaki, S.; Hidaka, J.; Shimura, Y. *Inorg. Chem.* **1973**, *12*, 142.
(2) Kaizaki, S.; Shimura, Y. *Bull. Chem. Soc. Jpn.* **1975**, *48*, 3611.
(3) Kaizaki, S.; Ito, M. *Bull. Chem. Soc. Jpn.* **1981**, *54*, 2499.
(4) Kaizaki, S.; Mori, H. *Bull. Chem. Soc. Jpn.* **1981**, *54*, 3562.
(5) Güdel, H. U.; Trabjerg, I.; Vala, M.; Ballhausen, C. J. *Mol. Phys.* **1972**, *24*, 1227.
(6) (a) McCarthy, P.; Vala, M. T. *Mol. Phys.* **1973**, *25*, 17. (b) Flint, C. D.; Matthews, A. P. *J. Chem. Soc., Faraday Trans. 2* **1976**, *72*, 576.
(7) Geiser, U.; Güdel, H. U. *Inorg. Chem.* **1981**, *20*, 3013.
(8) Peacock, R. D.; Stewart, B. *J. Chem. Soc., Chem. Commun.* **1982**, 295.
(9) Hilmes, G. L.; Brittain, H. G.; Richardson, F. S. *Inorg. Chem.* **1977**, *16*, 528.
(10) Jensen, H. P. *Acta Chem. Scand., Ser. A* **1981**, *A35*, 127.
(11) Harnung, S.; Laier, T. *Acta Chem. Scand., Ser. A* **1978**, *A32*, 41.
(12) Evans, R. S.; Schreiner, A. F.; Hauser, P. J. *Inorg. Chem.* **1974**, *13*, 2185.
(13) Mason, S. F. In "Fundamental Aspects and Recent Developments in Optical Rotatory Dispersion and Circular Dichroism"; Ciardelli, F., Salvadori, P., Eds.; Heyden and Son Ltd.: New York, 1973; p 196.
(14) Jensen, H. P. *Acta Chem. Scand., Ser. A* **1980**, *A34*, 355.

0020-1669/85/1324-2080$01.50/0

Table I. Analytical Data of the Complexes

complexes[a]	% C found	% C calcd	% H found	% H calcd	% N found	% N calcd
Λ-$(+)_{589}$-$[Cr(en)_2(R,R\text{-chxn})]Cl_3\cdot H_2O$ (C-II(2))	29.48	29.24	7.76	7.86	20.72	20.46
Δ-$(-)_{589}$-$[Cr(en)_2(R,R\text{-chxn})]Cl_3\cdot 0.75H_2O$ (C-III)	29.67	29.56	7.83	7.82	20.91	20.69
Δ-$(-)_{589}$-$[Cr(en)(R,R\text{-chxn})_2]Cl_3\cdot 4H_2O$ (C-IV)	31.96	32.41	8.33	8.55	16.00	16.20
Λ-$(+)_{589}$-$[Cr(en)_2(R\text{-pn})]Cl_3\cdot 3H_2O$ (P-II)	20.43	20.67	7.79	7.93	20.99	20.66
Δ-$(-)_{589}$-$[Cr(en)_2(R\text{-pn})]Cl_3\cdot H_2O\cdot 1.25NaCl$ (P-III)	18.52	18.95	6.34	6.36	18.67	18.94
Δ-$(-)_{589}$-$[Cr(en)(R\text{-pn})_2]Cl_3\cdot 1.5H_2O$ (P-IV)	23.90	24.40	7.78	7.94	21.49	21.34
Δ-$(-)_{589}$-$[Cr(R,R\text{-chxn})_3]Cl_3\cdot 4.5H_2O$ (C-V or I')	36.85	37.15	8.74	8.83	14.40	14.44
Δ-$(-)_{589}$-$[Cr(,R\text{-chxn})_2(S,S\text{-chxn})]Cl_3\cdot 4H_2O$ (II')	37.24	37.73	8.58	8.81	14.72	14.67
Δ-$(-)_{589}$-$[Cr(R,R\text{-chxn})(S,S\text{-chxn})_2]Cl_3\cdot 3.5H_2O$ (III')	38.24	38.32	8.58	8.77	14.93	14.90
Δ-$(-)_{589}$-$[Cr(S,S\text{-chxn})_3]Cl_3\cdot 1.5H_2O$ (IV')	41.55	40.95	8.68	8.59	15.71	15.91
Δ-$(-)_{589}$-$[Cr(R\text{-pn})_3]Cl_3\cdot 1.5H_2O$ (P-V or I)	26.05	26.51	7.95	8.16	20.71	20.61
Δ-$(-)_{589}$-$[Cr(R\text{-pn})_2(S\text{-pn})]Cl_3\cdot 0.5H_2O\cdot 0.75NaCl$ (II)	25.05	24.93	7.27	7.22	19.46	19.38
Δ-$(-)_{589}$-$[Cr(R\text{-pn})(S\text{-pn})_2]Cl_3\cdot 2H_2O\cdot 0.5NaCl$ (III)	23.63	23.75	7.70	7.76	18.10	18.47
Δ-$(-)_{589}$-$[Cr(S\text{-pn})_3]Cl_3\cdot 3H_2O$ (IV)	24.89	24.86	8.21	8.36	19.27	19.33
cis-$[Cr(NH_3)_2(en)_2]Br_3\cdot 0.5H_2O$	10.45	10.56	5.05	5.09	18.39	18.47
cis-$[Cr(NH_3)_2(S,S\text{-chxn})_2]Cl_3\cdot H_2O\cdot 3NaCl$	24.45	24.10	6.21	6.07	14.23	14.05
$[Cr(NH_3)_4(R\text{-pn})]Cl_3\cdot H_2O$	11.38	11.31	7.56	7.59	26.73	26.38

[a] The notations in the parentheses after the chemical formula are given as in the Experimental Section.

purpose, it seems valuable to study the room-temperature solution CD spectra of $Cr^{III}(N)_6$ type complexes with chiral diamines; the CD spectra may be separated into the configurational and vicinal CD curves. It is expected that the CD spectra in the spin-forbidden transitions are affected by conformational differences in diamine chelates as suggested previously.[6,7] Moreover, the vicinal CD curves, which may be calculated by adding or substracting the CD of diastereomeric pairs, will uncover more detailed CD components due to the electronic transitions than the configurational CD curves as found for (amino acidato)bis(ethylenediamine)-chromium(III) complexes.[3]

This paper deals with the preparation, characterization, and the CD spectra of the diastereomers of $[Cr(en)_x(diamine)_{3-x}]^{3+}$ (x = 0, 2), *cis*-$[Cr(NH_3)_2(diamine)_2]^{3+}$, and $[Cr(NH_3)_4(diamine)]^{3+}$, where the diamines used are (*R*)- or (*S*)-propylenediamine (*R*- or *S*-pn) and (1*R*,2*R*)- or (1*S*,2*S*)-1,2-*trans*-cyclohexanediamine (*R*,*R*- or *S*,*S*-chxn); among these complexes, four diastereomers of Λ-$[Cr(R\text{-pn})_x(S\text{-pn})_{3-x}]^{3+}$ and Λ-$[Cr(R,R\text{-chxn})_x(S,S\text{-chxn})_{3-x}]^{3+}$ are classified as the Λ-*lel*$_3$ (x = 0), Λ-*lel*$_2$*ob* (x = 1), Λ-*lelob*$_2$ (x = 2), and Λ-*ob*$_3$ (x = 3) isomers as described previously.[11] Further, the additivity and separability of the configurational and vicinal CD curves in the spin-forbidden and the first spin-allowed transitions are substantiated. On this basis, these CD spectra are elucidated in connection with the theoretical relations of the energy ordering and the rotational strengths between the spin-forbidden and the first spin-allowed transitions.

Experimental Section

Preparation of the Ligands. The chiral diamines were prepared by the methods described earlier: *R*- and *S*-pn;[15] *R*,*R*- and *S*,*S*-chxn.[16]

Preparation of the Complexes. The starting materials were prepared as described previously: *cis*-$[CrCl_2(en)_2]Cl$,[17] *trans*-$[CrF_2(R,R\text{-chxn})_2]ClO_4$,[18] $[Cr(NH_3)_5(H_2O)](ClO_4)_3$.[19]

(1) $[Cr(en)_x(R,R\text{-chxn})_{3-x}]Cl_3$ (x = 0–3). Two grams of finely powdered anhydrous *cis*-$[CrCl_2(en)_2]Cl$ and 0.9 g of anhydrous *R*,*R*-chxn were mixed together with a few drops of methyl cellosolve in a 25-mL beaker. This was covered with a watch glass and heated on a steam bath for 4–5 h until the color of the powder changed from purple to brown-yellow. Then, the reaction mixture was dried on a water bath. An aqueous solution of the obtained powder was poured into a column (2.5 × 150 cm) of SP Sephadex C-25 exchanger, and the charged complexes were eluted with a 0.2 M aqueous solution of sodium $(+)_{589}$-(tartrato)-antimonate(III) at a rate of 0.3 mL/min at 5 °C in the dark. The column gave five bands. Of these bands, the first (C-I) and the fifth (C-V) bands were found to be Λ-$(+)_{589}$-$[Cr(en)_3]^{3+}$ and Δ-$(-)_{589}$-$[Cr(R,R\text{-chxn})_3]^{3+}$ by means of the CD spectra in the first-band region. The ratios of the absorbance (A) to the CD absorbance differential ($\Delta A = A_L - A_R$) in the first-band region indicated that the second eluate (C-II) was impure in optical activity or configurational chirality and that the third (C-III) and the fourth (C-IV) eluates were pure. The C-II eluate was reloaded on a column of SP Sephadex C-25 exchanger and eluted with a 0.35 M NaH_2PO_4 solution at 5 °C in the dark. The column gave two bands. The faster band (C-II(1)) was found to be Δ-$(-)_{589}$-$[Cr(en)_3]^{3+}$ by the CD measurement. The slower band (C-II(2)) seemed to be one of the pure diastereomers of $[Cr(en)(R,R\text{-chxn})_2]^{3+}$ or $[Cr(en)_2(R,R\text{-chxn})]^{3+}$. After dilution of each eluate of the C-II(2), C-III, and C-IV bands with cold water at 5 °C, it was reloaded on a short column of SP Sephadex C-25 exchanger. Each adsorbed complex was washed thoroughly with a 0.05 M HCl solution and eluted with a 1 M HCl solution. Each eluate was evaporated to as small a volume as possible by a vacuum rotatory evaporator at about 30 °C. To each solution was added acetone, and then yellow powder was obtained. Each diastereomer was recrystallized from water and ethanol. The elemental analyses identified the C-II(2) and C-III complexes as $(+)_{589}$- and $(-)_{589}$-$[Cr(en)_2(R,R\text{-chxn})]^{3+}$, respectively, and also the C-IV one as $(-)_{589}$-$[Cr(en)(R,R\text{-chxn})_2]^{3+}$ as shown in Table I.

(2) $[Cr(en)_x(R\text{-pn})_{3-x}]Cl_3$ (x = 0–3). These complexes were prepared by a method similar to that for the corresponding *R*,*R*-chxn complexes as described above in (1). SP Sephadex column chromatography of the *R*-pn complexes showed the same behavior as for the *R*,*R*-chxn complexes except no formation of $(-)_{589}$-$[Cr(en)_3]^{3+}$ contaminating in the second eluate of the *R*,*R*-chxn complexes; the first (P-I), the fourth (P-IV), and the fifth (P-V) eluates from the column were found to be $(+)_{589}$-$[Cr(en)_3]^{3+}$, $(-)_{589}$-$[Cr(en)(R\text{-pn})_2]^{3+}$, and $(-)_{589}$-$[Cr(R\text{-pn})_3]^{3+}$, respectively. The second (P-II) and the third (P-III) bands correspond to $(+)_{589}$- and $(-)_{589}$-$[Cr(en)_2(R\text{-pn})]^{3+}$, respectively.

(3) $[Cr(R\text{-pn})_x(S\text{-pn})_{3-x}]Cl_3$. $(-)_{589}$-$[Cr(R\text{-pn})_3]^{3+}$ was obtained by the method of the preparation in (2). The other diastereomers were prepared by the modified methods described previously for $[Cr(en)_3]^{3+}$.[17-20] The SP Sephadex column chromatography of the products from *rac*-pn and $[CrCl_3(py)_3]$[20] or $CrCl_3\cdot 6H_2O$[21] in alcohol solutions gave three of four possible diastereomers; the *lel*$_3$, *lel*$_2$*ob*, and *lelob*$_2$ isomers. Under these preparative conditions, the most unstable *ob*$_3$ isomer could not be obtained. This complex was prepared by the reaction of anhydrous $CrCl_3$ in dimethyl sulfoxide (DMSO)[22] or in ether[23] at 35 °C as follows:

(a) A solution of 2 g of $CrCl_3\cdot 6H_2O$ in 4 mL of DMSO was boiled in a 20-mL beaker to obtain a red-violet solution. This was cooled to 30 °C, and a small amount of DMSO was added to prevent solidification upon cooling. To this solution was added 2 g of *R*-pn. The mixture was allowed to stand overnight at 35 °C. SP Sephadex column chromatography of this reaction mixture gave two bands. It was found that the faster and the slower eluates were the Λ-*lel*$_3$ and Δ-*ob*$_3$ isomers, respectively, by means of the CD spectra.

(b) To 3.5 g of anhydrous *rac*-pn in 20 mL of ether were added 2 g of anhydrous $CrCl_3$ and a small amount of zinc dust. The mixture was heated on a water bath for 2 days. After ether and unreacted *rac*-pn were

(15) "Shinjikken Kagaku Koza"; Maruzen: Tokyo, 1975; Vol. 8, p 1429.
(16) Galsbøl, F.; Steenbøl, P.; Sørensen, B. S. *Acta Chem. Scand.* **1972**, *26*, 3605.
(17) Pedersen, E. *Acta Chem. Scand.* **1970**, *24*, 3362.
(18) Glerup, J.; Josephsen, J.; Michelsen, K.; Pedersen, E.; Schäffer, C. E. *Acta Chem. Scand.* **1970**, *24*, 247.
(19) Linhard, M.; Berthod, W. *Z. Anorg. Allg. Chem.* **1955**, *276*, 173.
(20) Pfeiffer, P.; Haiman, M. *Ber. Dtsch. Chem. Ges.* **1903**, *36*, 1063.
(21) Gillard, R. D.; Mitchel, P. R. *Inorg. Synth.* **1972**, *13*, 2129.
(22) Glasbøl, A. F. G.; Harnung, S. E. *Acta Chem. Scand.* **1969**, *23*, 3027.
(23) Schläffer, H. L.; Kling, O. *Z. Anorg. Allg. Chem.* **1959**, *302*, 1.

Table II. Absorption Spectral Data of $[Cr(diamine)_3]^{3+}$, *cis*-$[Cr(NH_3)_2(diamine)_2]^{3+}$, and $[Cr(NH_3)_4(diamine)]^{3+}$

diamine	$\sigma/10^3$ cm^{-1} (ϵ/mol^{-1}·dm^3·cm^{-1})	
$(+)_{589}$-$(en)_2$(*R*,*R*-chxn)	21.8 (79.5)	28.6 (67.3)
$(-)_{589}$-$(en)_2$(*R*,*R*-chxn)	21.8 (85.5)	28.6 (75.2)
$(+)_{589}$-$(en)_2$(*R*-pn)	21.8 (72.8)	28.5 (59.5)
$(-)_{589}$-(*R*,*R*-chxn)$_3$	21.7 (83.4)	28.5 (66.3)
$(-)_{589}$-(*R*,*R*-chxn)$_2$(*S*,*S*-chxn)	21.7 (83.6)	28.5 (70.4)
$(-)_{589}$-(*R*,*R*-chxn)(*S*,*S*-chxn)$_2$	21.7 (81.2)	28.5 (70.1)
$(-)_{589}$-(*S*,*S*-chxn)$_3$	21.9 (85.5)	28.5 (72.9)
$(-)_{589}$-(*R*-pn)$_3$	21.7 (85.2)	28.6 (68.2)
$(-)_{589}$-(*R*-pn)$_2$(*S*-pn)	21.7 (77.8)	28.6 (63.6)
$(-)_{589}$-(*R*-pn)(*S*-pn)$_2$	21.8 (72.3)	28.6 (61.2)
$(-)_{589}$-(*S*-pn)$_3$	21.9 (73.5)	28.7 (63.4)
$(+)_{589}$-$(NH_3)_2(en)_2$	21.7 (63.9)	28.6 (52.6)
$(+)_{589}$-$(NH_3)_2$(*R*-pn)$_2$	21.6 (64.4)	28.5 (62.7)
$(-)_{589}$-$(NH_3)_2$(*R*-pn)$_2$	21.6 (65.3)	28.5 (66.7)
$(+)_{589}$-$(NH_3)_2$(*S*,*S*-chxn)$_2$	21.7 (61.2)	28.7 (89.6)
$(-)_{589}$-$(NH_3)_2$(*S*,*S*-chxn)$_2$	21.7 (71.8)	28.7 (101.9)
$(NH_3)_4$(*R*-pn)	21.7 (63.8)	28.7 (63.2)
$(NH_3)_4$(*R*,*R*-chxn)	21.9 (65.5)	28.7 (65.0)

discarded, the brown residue was dissolved in 0.1 HCl solution. SP Sephadex column chromatography of this solution gave four bands. In the elution order, the first (I), the second (II), the third (III), and the fourth (IV) eluates from the column were identified as the *lel*$_3$, *lel*$_2$*ob*, *lelob*$_2$, and *ob*$_3$ isomers, respectively. Each eluate was resolved into the enantiomers with use of SP Sephadex column chromatography by elution with 0.35 M aqueous solution of sodium $(+)_{589}$-(tartrato)antimonate(III); the faster and slower eluates are found to be Λ-$(+)_{589}$- and Δ-$(-)_{589}$ isomers, respectively.

(4) $[Cr(R,R\text{-chxn})_x(S,S\text{-chxn})_{3-x}]^{3+}$. The *lel*$_3$ isomer was obtained by preparation (1). The synthesis of the *ob*$_3$ isomer was attempted by the method of Harnung and Laier[11] several times, but this could not be obtained. This isomer was prepared not only by a method similar to that for Δ-$(-)_{589}$-$[Cr(R\text{-pn})_3]^{3+}$ but also by a method using *trans*-$[CrBr_2(R,R\text{-chxn})_2]Br$ as follows:

trans-$[CrBr_2(R,R\text{-chxn})_2]Br$ was prepared by dissolving *trans*-$[CrF_2(R,R\text{-chxn})_2]ClO_4$ in a concentrated HBr aqueous solution saturated with HBr at 0 °C. An equimolar amount of this dibromo complex and *S*,*S*-chxn was mixed in DMSO, and the mixture was allowed to stand overnight at 35 °C. The SP Sephadex column chromatography gave four bands. The first (I′), the second (II′), the third (III′), and the fourth (IV′) eluates were found to be the *lel*$_3$, *lel*$_2$*ob*, *lelob*$_2$, and *ob*$_3$ isomers, respectively, in elution order. This means that scrambling of the coordinated diamines and free diamines occurs during the formation of the tris(diamine) complexes. As a result, the obtained diastereomers became impure in optical activity or in configurational chirality. Each eluate was resolved into pure configurational isomers with use of SP Sephadex column chromatography by elution with a 0.2 M sodium $(+)_{589}$-tartrate solution. The faster and slower bands of each eluate were found to be $(+)_{589}$ and $(-)_{589}$ isomers, respectively.

(5) *cis*-$[Cr(NH_3)_2(en)_2]Br_3$. This was prepared by the reaction of *trans*-$[CrBr_2(en)_2]Br$ with liquid ammonia at room temperature as described earlier.[15] The product was found to be an almost cis isomer from the absorption spectrum as in Table II. This complex was resolved into enantiomers by SP Sephadex column chromatography by elution with a 0.2 M sodium $(+)_{589}$-(tartrato)antimonate(III) solution at 5 °C in the dark; equal amount of $(+)_{589}$- and $(-)_{589}$-*cis*-$[Cr(NH_3)_2(en)_2]^{3+}$ were eluted in this order.

(6) *cis*-$[Cr(NH_3)_2(R\text{-pn})_2]^{3+}$ and *cis*-$[Cr(NH_3)_2(R,R\text{-chxn})_2]^{3+}$. These complexes were obtained by the same method as that for *cis*-$[Cr(NH_3)_2(en)_2]^{3+}$ by using *trans*-$[CrBr_2(R\text{-pn})_2]Br$ and *trans*-$[CrBr_2(R,R\text{-chxn})_2]Br$ instead of *trans*-$[CrBr_2(en)_2]Br$. The optical resolution of these diastereomers was performed in the method similar to that for *cis*-$[Cr(NH_3)_2(en)_2]^{3+}$; the faster and the slower eluates from the SP Sephadex column are the $(+)_{589}$ and $(-)_{589}$ isomers, respectively. Isolation of each diastereomer of these complexes was unsuccessful, whereas the diastereomeric mixture of the *R*,*R*-chxn complex was isolated as a solid.

(7) $[Cr(NH_3)_4(R\text{-pn})]^{3+}$ and $[Cr(NH_3)_4(R,R\text{-chxn})]^{3+}$. To 3 g of $[Cr(NH_3)_5(H_2O)](ClO_4)_3$ in 30 mL of DMSO was added dropwise 0.4 g of anhydrous *R*-pn or *R*,*R*-chxn in 5 mL of DMSO with stirring. The mixture was allowed to stand for 1 week at 4–10 °C. After the reaction mixture was neutralized with a dilute HCl solution, the solution was charged on a column of SP Sephadex C-25 exchanger. The adsorbed complexes were eluted with a 0.3 M NaCl solution. The column gave two bands for the *R*-pn complexes and one band for the *R*,*R*-chxn complexes. The faster eluate was found to be $[Cr(R\text{-pn})_3]^{3+}$. The remaining slower eluate of the *R*-pn complexes and only one eluate of the *R*,*R*-chxn complexes seem to $[Cr(NH_3)_4(R\text{-pn})]^{3+}$ and $[Cr(NH_3)_4(R,R\text{-chxn})]^{3+}$, respectively. $[Cr(NH_3)_4(R\text{-pn})]Cl_3\cdot H_2O$ was isolated by the procedure using SP Sephadex column chromatography as described in preparation (1) and confirmed by elemental analyses as in Table I. Isolation of the *R*,*R*-chxn complex failed.

Measurements. Absorption spectra were obtained by a Shimadzu UV-200S spectrophotometer. CD spectra were recorded with a Jasco MOE-1 spectropolarimeter. All the measurements were carried out in aqueous solutions at room temperature. The quantitative absorption and CD spectra of $(+)_{589}$- and $(-)_{589}$-*cis*-$[Cr(NH_3)_2(R\text{-pn})_2]^{3+}$ and $[Cr(NH_3)_4(R,R\text{-chxn})]^{3+}$ were obtained on the basis of quantitative analyses of Cr^{3+} content in the sample solution eluted from the SP Sephadex column with a 2 M LiCl solution. It was found that there is no difference in the CD spectrum of $(+)_{589}$-*cis*-$[Cr(NH_3)_2(en)_2]^{3+}$ in H_2O and that in a 2 M LiCl solution.

Results and Discussion

Preparation and Characterization of the Complexes. $[Cr(en)_2(diamine)]^{3+}$. The reaction of *cis*-$[CrCl_2(en)_2]Cl$ with anhydrous *R*-diamine without solvents gave almost the diastereomers of $[Cr(en)_2(R\text{-diamine})]^{3+}$, whereas the addition of a small amount of methyl cellosolve promoted the formation of $[Cr(en)(R\text{-diamine})_2]^{3+}$, $[Cr(en)_3]^{3+}$, and $[Cr(R\text{-diamine})_3]^{3+}$; the scrambling of the diamines within the complexes easily occurs under rather homogeneous conditions. It is to be noted that the formation ratio of Λ-$(+)_{589}$- and Δ-$(-)_{589}$-$[Cr(en)_3]^{3+}$ is not unity but 1.6 for the *R*-pn case and that the Λ-$(+)_{589}$ enantiomer is exclusively formed for the *R*,*R*-chxn case as mentioned in Experimental Section. Such a predominant formation of the Λ enantiomer may result from the easiness of the displacement of an *R*-diamine ligand in unstable Λ-(*ob*)-$[Cr(en)_2(R\text{-diamine})]^{3+}$ by free ethylenediamine released from Δ-*lel*-$[Cr(en)_2(R\text{-diamine})]^{3+}$ and/or Δ-*lel*$_2$-$[Cr(en)(R\text{-diamine})_2]^{3+}$ when attacked by free *R*-diamine.

The absolute configuration of two diastereomers of $[Cr(en)_2(R\text{-diamine})]^{3+}$ is determined to be Λ and Δ for the faster (C-II(2) and P-II) and the slower eluates (C-III and P-III), respectively, on the basis of the major CD band in the first spin-allowed transitions as shown in Figure 1.

$[Cr(R\text{-diamine})_x(S\text{-diamine})_{3-x}]^{3+}$. The absorption and CD spectra of four diastereomers of Λ-$[Cr(R,R\text{-chxn})_x(S,S\text{-chxn})_{3-x}]^{3+}$ are found to agree with those reported by Harnung and Laier[11] as shown in Table II and Figure 2. According to their assignments,[11] therefore, the first (C-V or I′), the second (II′), the third (III′), and the fourth (IV′) eluates from the column are identified as the *lel*$_3$, *lel*$_2$*ob*, *lelob*$_2$, and *ob*$_3$ isomers, respectively. Since the CD behavior of each of the four diastereomers of Λ-$[Cr(R\text{-pn})_x(S\text{-pn})_{3-x}]^{3+}$ is similar to that of the corresponding diastereomers of Λ-$[Cr(R,R\text{-chxn})_x(S,S\text{-chxn})_{3-x}]^{3+}$ as in Figure 2, the first (P-V or I), the second (II), the third (III), and the fourth (IV) eluates from the column are assigned to the *lel*$_3$, *lel*$_2$*ob*, *lelob*$_2$, and *ob*$_3$ isomers, respectively as summarized in Table I. No attempt was made to separate nine meridional and three facial geometrical isomers of Λ-$[Cr(R\text{-pn})_x(S\text{-pn})_{3-x}]^{3+}$ with respect to methyl groups on propylenediamine ligands. It has been revealed that there is no virtual influence of such geometrical isomerism on the CD spectra of the corresponding cobalt(III) complexes, $[Co(R\text{-pn})_x(S\text{-pn})_{3-x}]^{3+}$.[24] Hence, it can be assumed that meridional and facial isomers of the Cr(III) complexes give almost identical CD spectra.

***cis*-$[Cr(NH_3)_2(diamine)_2]^{3+}$.** The visible absorption spectra (Table II) and the optical resolution by SP Sephadex column chromatography indicate that the syntheses of the *cis*-diamine-bis(diamine) complexes involve the trans → cis isomerization as pointed out previously.[25] The chromatographic behavior for the optical resolution of either of the bis(diamine) complexes is the same as that of the tris(diamine) complexes; the faster and slower eluates are found to take a Λ and Δ absolute configurations, respectively, from the CD spectra in the first-band region as in

(24) Harnung, S. E.; Kallesøe, S.; Sargeson, A. M.; Schäffer, C. E. *Acta Chem. Scand., Ser. A* **1974**, *A28*, 385.
(25) Wong, C. F. C.; Kirk, A. D. *Inorg. Chem.* **1978**, *17*, 1672.

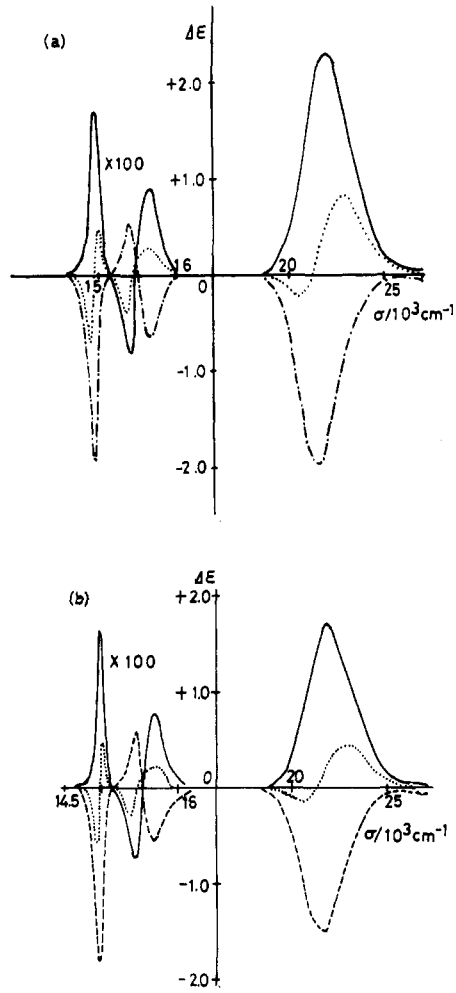

Figure 1. CD spectra of $[Cr(en)_2(diamine)]^{3+}$: (a) *R*-pn, Λ-$(+)_{589}$ isomer (P-II eluate) (—), Δ-$(-)_{589}$ isomer (P-III eluate) (-·-); (b) *R*,*R*-chxn, Λ-$(+)_{589}$ isomer (C-II(2)) (—), Δ-$(-)_{589}$ isomer (C-III) (---). The dotted curves in both (a) and (b) indicate the vicinal CD curves $[\Delta\epsilon(\Lambda$ *R*-diamine) + $\Delta\epsilon(\Delta$ *R*-diamine) = $2\Delta\epsilon$(*R*-diamine)].

Figure 3. Three possible geometrical isomers with respect to methyl groups on *R*-pn of Λ-$[Cr(NH_3)_2(R\text{-pn})_2]^{3+}$ are also disregarded for the same reason as in the case of the $(pn)_3$ complexes.

$[Cr(NH_3)_4(diamine)]^{3+}$. Wong and Kirk prepared $[Cr(NH_3)_4(en)](ClO_4)_3\cdot H_2O$ through a five-stage synthesis with use of $[Cr(NH_3)(en)(O_2)_2]\cdot H_2O$ as a starting complex.[25] While this procedure is very tedious, our new preparation method for the tetraammine complexes is very simple and applicable to the complexes with other diamines.

CD Spectra of the Tris- and Bis(diamine) Complexes. The CD spectrum of Λ-$(+)_{589}$-$[Cr(en)_3]^{3+}$ in the spin-forbidden transitions at room temperature was remeasured as in Figure 4. Three CD peaks are more distinct than that observed previously,[1] but close to the reported one.[9] The assignment of the three CD peaks in the spin-forbidden transitions is confirmed on the basis of the recent analyses of single-crystal CD spectra[7,14] as in Table III. The curve analyses for these distinct CD peaks give the experimental ratios of the rotational strengths for the three transitions; i.e., $R(^2E(^2E_g)):R(^2A_2(^2T_{1g})):R(^2E(^2T_{1g}))$ is found to be 1:-0.81:1.07. From this result, the ratio of the rotational strengths for the trigonal split components in the first spin-allowed transitions may be estimated according to eq 1a–c, giving the theoretical

$$R(^2E(^2E_g)) = 32k[R(^4E) + R(^4A_1)] \quad (1a)$$

$$R(^2A_2(^2T_{1g})) = 2k[R(^4E) + 4R(^4A_1)] \quad (1b)$$

$$R(^2E(^2T_{1g})) = 2k[5R(^4E) + 2R(^4A_1)] \quad (1c)$$

relations between the rotational strengths for the spin-forbidden transitions and those for the first spin-allowed transitions as described previously.[1] k is equal to $\zeta'^2/18[E(^4T_{2g}) - E(^2\Gamma)]^2$, where ζ' is the spin–orbit coupling constant and $E(^4T_{2g}) - E(^2\Gamma)$ stands for the energy interval between the $^4T_{2g}$ and the doublet $(^2\Gamma)$ states concerned. By using the above equations, the ratios of the rotational strengths for the trigonal components, $R(^4E):R(^4A_1)$, are found to be −1.22, −1.15, and −1.30 from the ratios $R(^2E(^2E_g)):R(^2A_2(^2T_{1g})) = -1.24$, $R(^2E(^2T_{1g})):R(^2A_2(^2T_{1g})) = -1.31$, and $R(^2E(^2T_{1g})):R(^2E(^2E_g)) = 1.07$, respectively. These values of $R(^4E):R(^4A_1)$ are in fair agreement with each other and with the theoretical value.[12] However, they disagree with the experimental ratio of −2 obtained from the single-crystal CD study.[14] From the ratio, $R(^4E):R(^4A_1) = -2$, the predicted ratios of the rotational strengths for the spin-forbidden transitions are estimated

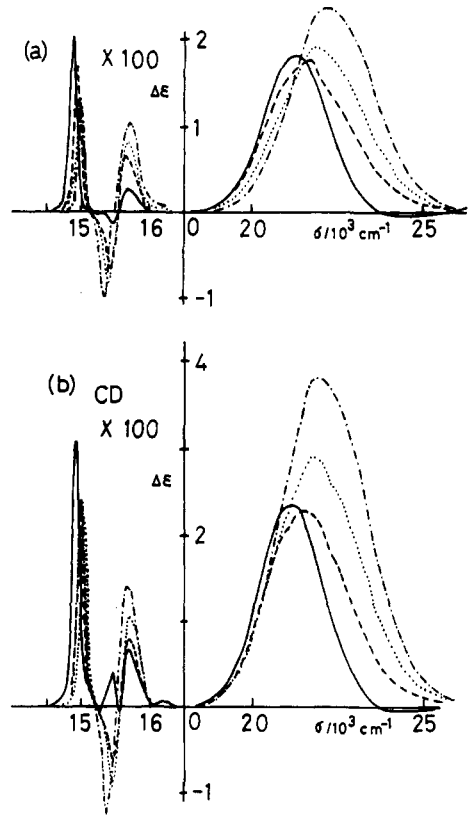

Figure 2. CD spectra of Λ-$[Cr(diamine)_3]^{3+}$: (a) Λ-$[Cr(R\text{-pn})_x(S\text{-pn})_{3-x}]^{3+}$; (b) Λ-$[Cr(R,R\text{-chxn})_x(S,S\text{-chxn})_{3-x}]^{3+}$. Key: $x = 3$ (lel_3) (—); $x = 2$ (lel_2ob) (···); $x = 1$ ($lelob_2$) (---); $x = 0$ (ob_3) (-·-).

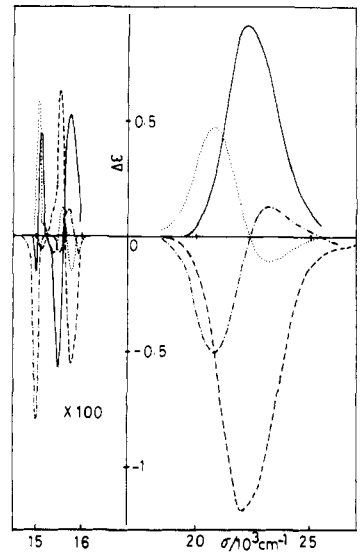

Figure 3. CD spectra of *cis*-$[Cr(NH_3)_2(diamine)_2]^{3+}$: *cis*-$[Cr(NH_3)_2(R\text{-pn})_2]^{3+}$ [Δ-$(-)_{589}$ isomer (-··-), Λ-$(+)_{589}$ isomer (—)]; *cis*-$[Cr(NH_3)_2(R,R\text{-chxn})_2]^{3+}$ [Δ-$(-)_{589}$ isomer (···), Λ-$(+)_{589}$ isomer (---)].

Table III. Configurational CD Data of Λ-$[Cr(en)_x(diamine)_y(NH_3)_z]^{3+}$ Type Complexes

complex	$\sigma/10^3$ cm^{-1} ($\Delta\epsilon$/mol^{-1}·dm^3·cm^{-1})[a]		assgnt
$(+)_{589}$-$[Cr(en)_3]^{3+}$	14.93 (+1.62*)		$^2E(^2E_g)$
	15.42 (−0.64*)		$\bar{E}_b(^2A_2(^2T_{1g}))$
	15.72 (+0.65*)		$2\bar{A}$, $\bar{E}_a(^2E(^2T_{1g}))$
	22.03 (+1.64)		$^4E(^4T_{2g})$
	28.57 (−0.01)		
	30.68 (+0.07)		
	$^1/_2\{lel_3 + ob_3\}$ (eq 2a)	$^1/_2\{lel_2ob + lelob_2\}$ (eq 2b)	
$[Cr(R\text{-pn})_x(S\text{-pn})_{3-x}]^{3+}$	14.90 (+1.06*)	15.00 (+1.31*)	$^2E(^2E_g)$
	15.40 (−0.51*)	15.45 (−0.69*)	$\bar{E}_b(^2A_2(^2T_{1g}))$
	15.70 (+0.66*)	15.70 (+0.72*)	$2\bar{A}$, $\bar{E}_a(^2E(^2T_{1g}))$
	21.70 (+1.90)	21.70 (+1.85)	$^4E(^4T_{2g})$
	28.40 (−0.05)	28.20 (−0.04)	
	30.20 (+0.04)	30.20 (+0.05)	
	$^1/_2\{lel_3 + ob_3\}$ (eq 2a)	$^1/_2\{lel_2ob + lelob_2\}$ (eq 2b)	
$[Cr(R,R\text{-chxn})_x(S,S\text{-chxn})_{3-x}]^{3+}$	15.00 (+1.61*)	15.00 (+2.12*)	$^2E(^2E_g)$
	15.35 (−0.51*)	15.45 (−0.75*)	$\bar{E}_b(^2A_2(^2T_{1g}))$
	15.70 (+1.03*)	15.70 (+0.92*)	$2\bar{A}$, $\bar{E}_a(^2E(^2T_{1g}))$
	21.70 (+2.86)	21.70 (+2.59)	$^4E(^4T_{2g})$
	28.10 (−0.009)	28.10 (−0.005)	
	30.50 (+0.056)	29.90 (+0.006)	
	$^1/_2\{\Delta\text{-}(R\text{-pn}) - \Lambda\text{-}(R\text{-pn})\}$	$^1/_2\{\Delta\text{-}(R,R\text{-chxn}) - \Lambda\text{-}(R,R\text{-chxn})\}$	
$[Cr(en)_2(R\text{-diamine})]^{3+}$	14.97 (+1.69*)	14.93 (+1.76*)	$^2E(^2E_g)$
	15.43 (−0.64*)	15.41 (−0.63*)	$\bar{E}_b(^2A_2(^2T_{1g}))$
	15.70 (+0.67*)	15.65 (+0.75*)	$2\bar{A}$, $\bar{E}_a(^2E(^2T_{1g}))$
	21.83 (+1.61)	21.79 (+2.12)	$^4E(^4T_{2g})$
	28.33 (−0.02)	28.28 (+0.01)	
	30.49 (+0.06)	20.20 (+0.07)	
	$^1/_2\{\Lambda\text{-}(R\text{-pn}_2) - \Delta\text{-}(R\text{-pn}_2)\}$	$^1/_2\{\Lambda\text{-}(R,R\text{-chxn}_2) - \Delta\text{-}(R,R\text{-chxn}_2)\}$	
cis-$[Cr(NH_3)_2(diamine)_2]^{3+}$	15.05 (+0.37*)	15.11 (+0.35*)	
	15.48 (−0.25*)	15.53 (−0.26*)	
	15.82 (+0.23*)	15.82 (+0.19*)	
	22.00 (+0.51)	21.75 (+0.65)	
	26.25 (+0.03)	26.25 (+0.04)	
	28.50 (−0.01)	30.00 (+0.02)	
	30.25 (+0.08)		
$(+)_{546}$-*cis*-$[Cr(NH_3)_2(en)_2]^{3+}$	15.08 (+0.51*)		
	15.57 (−0.21*)		
	15.85 (+0.25*)		
	21.85 (+0.51)		
	26.50 (+0.038)		
	30.25 (+0.026)		

[a] Asterisked CD intensities are multiplied by 10^2.

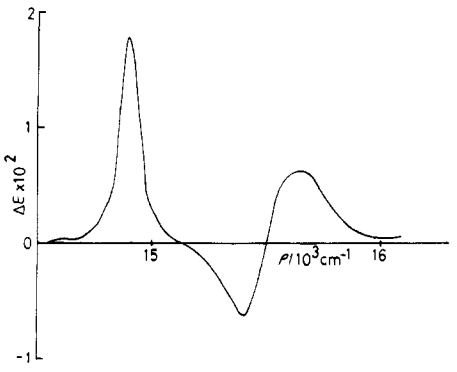

Figure 4. CD spectrum in the spin-forbidden transitions of Λ-$(+)_{589}$-$[Cr(en)_3]^{3+}$ at room temperature in H_2O.

to be $R(^2E(^2E_g)):R(^2A_2(^2T_{1g})):R(^2E(^2T_{1g})) = 8:-1:3$ by using eq 1a–c. This is very similar to the ratios of the CD intensities in the spin-forbidden transitions of Λ-*lel*$_3$-$[Cr(S\text{-pn})_3]^{3+}$ in solution as in Figure 2. The discrepancy of the experimental values of $R(^4E):R(^4A_1)$ may be ascribed to the differences in the CD contributions from ethylenediamine chelate conformations in crystals (predominantly *lel*$_3$) and in solutions (presumably a greater abundance of *lel*$_2$*ob*) of $[Cr(en)_3]^{3+}$. In view of this quantitative treatment, our theoretical approach seems appropriate for the elucidation of the CD behavior in the spin-forbidden transitions.

The CD spectra of Λ-$[Cr(R\text{-pn})_x(S\text{-pn})_{3-x}]^{3+}$ and Λ-$[Cr(R,R\text{-chxn})_x(S,S\text{-chxn})_{3-x}]^{3+}$ vary regularly with the diastereomers as in Figure 2. That is, the CD intensities in the first spin-allowed transitions near 21 000 cm^{-1} decrease in the order of the *ob*$_3$, *lelob*$_2$, *lel*$_3$, and *lel*$_2$*ob* complexes, and those of the lowest frequency CD peak in the spin-forbidden transitions near 15 000 cm^{-1} increase in the order of the *ob*$_3$, *lelob*$_2$, *lel*$_2$*ob*, and *lel*$_3$ complexes in the cases of both diamines. The CD positions in the first-band region shift to the higher frequency side in increasing order of the lel conformations in the complexes. More drastic CD changes are observed in both the spin-forbidden and the first spin-allowed band region on going from the *lel*$_2$ to *ob*$_2$ *cis*-diamminebis(diamine) complexes as in Figure 3. In contrast, there are small differences in the CD patterns of the diastereomers of $[Cr(en)_2(diamine)]^{3+}$ as shown in Figure 1. Most of the tris(diamine) complexes and the two diastereomers of $[Cr(en)_2(diamine)]^{3+}$ give three CD peaks in the spin-forbidden band region, while more than three CD peaks are observed for Λ-*lel*$_3$-$[Cr(S,S\text{-chxn})_3]^{3+}$ and most of *cis*-$[Cr(NH_3)_2(diamine)_2]^{3+}$. In view of the inversion of the CD signs of the $^2T_{1g}$ split components for Λ-*lel*$_3$- and Δ-*ob*$_3$-$[Cr(S,S\text{-chxn})_3]^{3+}$, Harnung and Laier claimed that the energy ordering of the $^2T_{1g}$ components of the former *lel*$_3$ complex is reverse to that of the latter *ob*$_3$ complex and $[Cr(en)_3]^{3+}$.[11] However, it is unlikely that the complexes with almost identical chromophores have such different electronic excited states as to reverse the energy ordering. It is rather more plausible that such complicated CD behavior in the spin-forbidden transitions arises from the vibronic structure and/or the superposition of the configurational con-

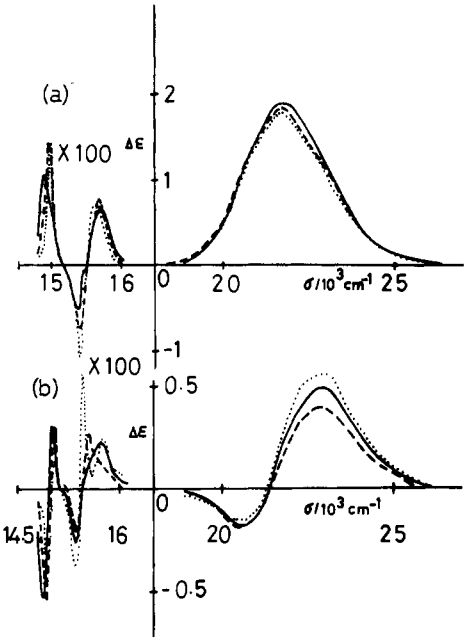

Figure 5. Configurational (a) and vicinal (b) CD curves of Λ-[Cr(*R*-pn)$_x$(*S*-pn)$_{3-x}$]$^{3+}$: (a) calculated from eq 2a (—), 2b (---), and 2c (···); (b) calculated from eq 3a (—), 3b (---), and 3c (···).

tribution due to chirality around metal ions and the vicinal one due to chirality on ligands. The above regular variation of the CD behavior among the diastereomers suggests that the superposition of the configurational and vicinal CD contributions is most probable. Thus, the separation of these contributions is attempted by adding and substracting the observed CD spectra of pairs of the diastereomers according to the equations

$$\Delta\epsilon(\Lambda) = \tfrac{1}{2}\{\Delta\epsilon(lel_3) + \Delta\epsilon(ob_3)\} \quad (2a)$$

$$\Delta\epsilon(\Lambda) = \tfrac{1}{2}\{\Delta\epsilon(lel_2ob) + \Delta\epsilon(lelob_2)\} \quad (2b)$$

$$\Delta\epsilon(\Lambda) = \tfrac{1}{2}\{3\Delta\epsilon(lel_2ob) - \Delta\epsilon(lel_3)\} \quad (2c)$$

$$\Delta\epsilon(R\text{-diamine}) = \tfrac{1}{6}\{\Delta\epsilon(ob_3) - \Delta\epsilon(lel_3)\} \quad (3a)$$

$$\Delta\epsilon(R\text{-diamine}) = \tfrac{1}{2}\{\Delta\epsilon(lelob_2) - \Delta\epsilon(lel_2ob)\} \quad (3b)$$

$$\Delta\epsilon(R\text{-diamine}) = \tfrac{1}{2}\{\Delta\epsilon(ob_3) - \Delta\epsilon(lelob_2)\} \quad (3c)$$

where the CD curves of the diastereomers are assumed as follows:

$$\Delta\epsilon(lel_3) = \Delta\epsilon(\Lambda) - 3\Delta\epsilon(R\text{-diamine})$$

$$\Delta\epsilon(lel_2ob) = \Delta\epsilon(\Lambda) - \Delta\epsilon(R\text{-diamine})$$

$$\Delta\epsilon(lelob_2) = \Delta\epsilon(\Lambda) + \Delta\epsilon(R\text{-diamine})$$

$$\Delta\epsilon(ob_3) = \Delta\epsilon(\Lambda) + 3\Delta\epsilon(R\text{-diamine})$$

Each configurational ($\Delta\epsilon(\Lambda)$) and vicinal ($\Delta\epsilon(R$-diamine)) CD is calculated by using two sets of three different equations: (2a)–(2c) and (3a)–(3c), respectively. Each calculated CD curve is similar to the others as shown in Figures 5 and 6 and Table III; the configurational CD curves give only one band in the first spin-allowed transitions and three peaks in the spin-forbidden transitions, whereas the vicinal CD curves show two bands in the former region and four peaks in the latter region. The similar CD patterns are obtained from the CD spectra of the diastereomeric pairs of [Cr(en)$_2$(diamine)]$^{3+}$ and *cis*-diamminebis(*R*-diamine) complexes as shown in Figures 1, 4, 7, and 8 and Tables III–V. Since the configurational CD curves agree with the CD spectra of the parent complexes such as (+)$_{589}$-[Cr(en)$_3$]$^{3+}$ and (+)$_{589}$-*cis*-[Cr(NH$_3$)$_2$(en)$_2$]$^{3+}$, the configurational and vicinal CD effects are additive and separable in both the spin-forbidden and the first spin-allowed transitions of the present complexes. Accordingly, it is seen that the complicated CD patterns in the spin-forbidden transitions of the diastereomers result in the superposition of the configurational and vicinal CD effects. This manifests the accuracy and reliability of the present measurements for the weak but sharp CD peaks in spite of using a commercially available CD instrument with ordinary sensitivity and wavelength precision.

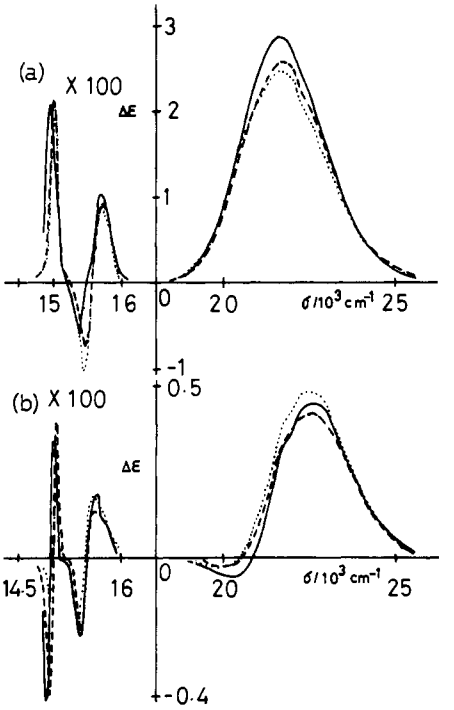

Figure 6. Configurational (a) and vicinal (b) CD curves of Λ-[Cr(*R*,*R*-chxn)$_x$(*S*,*S*-chxn)$_{3-x}$]$^{3+}$: (a) calculated from eq 2a (—), 2b (---), and 2c (···); (b) calculated from eq 3a (—), 3b (---), and 3c (···).

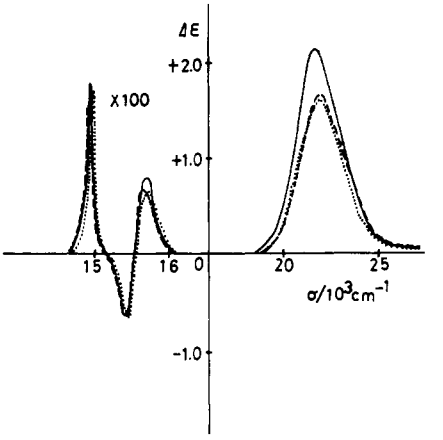

Figure 7. Configurational CD curves of Λ-[Cr(en)$_2$(diamine)]$^{3+}$ [$^1/_2${Δε(Λ *R*-diamine) − Δε(Δ *R*-diamine)} = Δε(Λ)]: *R*,*R*-chxn (—); *R*-pn (···); en (---).

Three configurational CD peaks in the spin-forbidden transitions of the tris- and bis(diamine) complexes can be assigned in the case of the (en)$_3$ complex as in Table III. Among four vicinal CD peaks in the spin-forbidden transitions, two higher frequency peaks are located at the position close to the $^2T_{1g}$ split components of the configurational CD curves as shown in Figures 4–6 and 8 and Tables III–V. Thus, these CD peaks are unambiguously assigned to the $^2A_2(^2T_{1g})$ and $^2E(^2T_{1g})$ components from the lower frequency side. The remaining vicinal CD peaks at the lower frequency side are covered under the band envelope of the lowest frequency $^2E(^2E_g)$ configurational CD peak as shown in Figures 4–6 and 8 and Tables III–V. To ensure that these two CD components correspond to the electronic transitions to the Kramers doublets ($\bar{E}$ and $2\bar{A}$) of the ^2E_g state as revealed by the low-temperature single-crystal spectroscopic studies,[5-8] the CD signs and the energy ordering of these peaks are examined in terms of the following

Table IV. Vicinal CD Data of $[Cr(en)_x(diamine)_{3-x}]^{3+}$ Type Complexes

complex	$\sigma/10^3$ cm^{-1} ($\Delta\epsilon$/mol^{-1}·dm^3·cm^{-1})[a]		assgnt
	$^1/_6\{lel_3 - ob_3\}$ (eq 3a)	$^1/_2\{lelob_2 - lel_2ob\}$ (eq 3b)	
$[Cr(R\text{-pn})_x(S\text{-pn})_{3-x}]^{3+}$	14.90 (−0.30*)	14.95 (−0.33*)	$2\bar{A}(^2E_g)$
	15.00 (+0.16*)	15.05 (+0.18*)	$\bar{E}(^2E_g)$
	15.35 (−0.16*)	15.40 (−0.12*)	$\bar{E}_b(^2A_2(^2T_{1g}))$
	15.65 (+0.13*)	15.55 (+0.16*)	$2\bar{A}, \bar{E}_a(^2E(^2T_{1g}))$
	20.60 (−0.11)	20.50 (−0.11)	$^4A_1(^4T_{2g})$
	23.00 (+0.29)	22.80 (+0.24)	$^4E(^4T_{2g})$
	28.20 (−0.05)	28.60 (−0.06)	
$[Cr(R,R\text{-chxn})_x(S,S\text{-chxn})_{3-x}]^{3+}$	14.90 (−0.42*)	14.90 (−0.40*)	$2\bar{A}(^2E_g)$
	15.00 (+0.27*)	15.05 (+0.40*)	$\bar{E}(^2E_g)$
	15.40 (−0.23*)	15.40 (−0.21*)	$\bar{E}_b(^2A_2(^2T_{1g}))$
	15.60 (+0.15*)	15.60 (+0.14*)	$2\bar{A}, \bar{E}_a(^2E(^2T_{1g}))$
	19.80 (−0.06)	19.80 (−0.02)	$^4A_1(^4T_{2g})$
	22.60 (+0.45)	22.60 (+0.43)	$^4E(^4T_{2g})$
	28.10 (−0.03)	28.10 (−0.05)	
	$^1/_2\{\Delta\text{-}(R\text{-pn}) + \Lambda\text{-}(R\text{-pn})\}$	$^1/_2\{\Delta\text{-}(R,R\text{-chxn}) + \Lambda\text{-}(R,R\text{-chxn})\}$	
$[Cr(en)_2(R\text{-diamine})]^{3+}$	14.95 (−0.26*)	14.88 (−0.34*)	$2\bar{A}(^2E_g)$
	15.02 (+0.23*)	14.99 (+0.24*)	$\bar{E}(^2E_g)$
	15.41 (−0.16*)	15.36 (−0.19*)	$\bar{E}_b(^2A_2(^2T_{1g}))$
	15.72 (+0.12*)	15.63 (+0.15*)	$2\bar{A}, \bar{E}_a(^2E(^2T_{1g}))$
	20.41 (−0.07)	20.58 (−0.10)	$^4A_1(^4T_{2g})$
	22.95 (+0.23)	22.94 (+0.42)	$^4E(^4T_{2g})$
	28.50 (−0.04)	28.20 (−0.04)	
	$^1/_4\{\Delta\text{-}(R\text{-pn}_2) + \Lambda\text{-}(R\text{-pn}_2)\}$	$^1/_4\{\Delta\text{-}(R,R\text{-chxn}_2) + \Lambda\text{-}(R,R\text{-chxn}_2)\}$	
cis-$[Cr(NH_3)_2(R\text{-diamine})_2]^{3+}$	15.02 (−0.22*)	15.04 (−0.15*)	$2\bar{A}(^2E_g)$
	15.10 (+0.09*)	15.15 (+0.08*)	$\bar{E}(^2E_g)$
	15.48 (−0.16*)	15.53 (−0.18*)	$\bar{E}_b(^2A_2(^2T_{1g}))$
	15.75 (+0.16*)	15.77 (+0.17*)	$2\bar{A}, \bar{E}_a(^2E(^2T_{1g}))$
	20.25 (−0.08)	20.00 (−0.05)	$^4A_1(^4T_{2g})$
	22.75 (+0.24)	22.75 (+0.29)	$^4E(^4T_{2g})$
	28.75 (−0.03)	28.00 (−0.005)	

[a] Asterisked CD intensities are multiplied by 10^2.

Table V. Vicinal CD Data of *cis*-Diamminebis(diamine) and Tetraammine Complexes

complex	$\sigma/10^3$ cm^{-1} ($\Delta\epsilon$/mol^{-1}·dm^3·cm^{-1})[a]		assgnt
	$^1/_4\{\Delta\text{-}(R\text{-pn}_2) + \Lambda\text{-}(R\text{-pn}_2)\}$	$^1/_4\{\Delta\text{-}(R,R\text{-chxn}_2) + \Lambda\text{-}(R,R\text{-chxn}_2)\}$	
cis-$[Cr(NH_3)_2(diamine)_2]^{3+}$	15.02 (−0.22*)	15.04 (−0.15*)	$^2B_1(^2E_g)$
	15.10 (+0.09*)	15.15 (+0.18*)	$^2A_1(^2E_g)$
	15.48 (−0.16*)	15.53 (−0.18*)	$^2E(^2T_{1g})$
	15.75 (+0.16*)	15.77 (+0.17*)	$^2A_2(^2T_{1g})$
	20.25 (−0.08)	20.00 (−0.05)	$^4B_2(^4T_{2g})$
	22.75 (+0.24)	22.75 (+0.29)	$^4E(^4T_{2g})$
	28.75 (−0.03)	28.00 (−0.005)	
	R-pn	*R,R*-chxn	
$[Cr(NH_3)_4(diamine)]^{3+}$	15.13 (−0.12*)	15.04 (−0.36*)	$^2A_1(^2E_g)$
	15.23 (+0.17*)	15.15 (+0.07*)	$^2B_1(^2E_g)$
	15.53 (+0.13*)	15.38 (+0.16*)	$^2E(^2T_{1g})$
	15.65 (−0.16*)	15.80 (−0.14*)	$^2A_2(^2T_{1g})$
	15.85 (+0.18*)		unidentified
	20.00 (−0.05)	20.00 (−0.09)	$^4E(^4T_{2g})$
	22.25 (+0.22)	22.50 (+0.26)	$^4B_2(^4T_{2g})$
	28.50 (−0.01)	28.50 (−0.06)	

[a] Asterisked CD intensities are multiplied by 10^2.

theoretical approaches. As described previously,[1] the rotational strengths for the spin-forbidden transitions to the Kramers doublets of the ^2E_g state can be represented as

$$R(\bar{E}) = 4k[5R(^4E) + 2R(^4A_1)] \quad (4a)$$

$$R(2\bar{A}) = 4k[3R(^4E) + 6R(^4A_1)] \quad (4b)$$

where k is given as in eq 1a–c. Since the rotational strengths for the $\bar{E}(^2E_g)$ and $2\bar{A}(^2E_g) \leftarrow {}^4A_2$ transitions are contributed largely from those for the $^4\bar{E}(^4T_{2g})$ and $^4A_1(^4T_{2g}) \leftarrow {}^4A_2$ transitions, respectively, as in eq 4a and b, the CD signs of the $\bar{E}$ and $2\bar{A}$ components depend on the assignments of the two vicinal CD bands in the first spin-allowed transitions. In the case of the vicinal CD curves due to the *R*-diamine ligands, negative and positive bands in the first-band region are assigned to the $^4A_1$ and ^4E components from the lower frequency side, respectively, by using eq 1b and c, because the $^2A_2(^2T_{1g})$ and $^2E(^2T_{1g})$ vicinal CD components are found to be negative and positive, respectively, as mentioned above. This assignment of the CD in the first-band region agrees with the result from the single-crystal absorption and CD spectra.[6a,8] Therefore, the $2\bar{A}$ and $\bar{E}$ CD peaks are predicted to give negative and positive signs, respectively, according to eq 4a and b. The energy ordering for these peaks can be considered from eq 5, which is derived with use of Sugano–

$$E(2\bar{A}) - E(\bar{E}) = 4K\zeta'/[E(^2E) - E(^2T_1)] \quad (5)$$

Tanabe's perturbation theory,[26] where K is the trigonal splitting parameter that refers to the energy interval of the $^4T_{2g}$ state in a trigonal field, $^2/_3[E(^4E) - E(^4A_1)]$. The denominator of eq 5

(26) Sugano, S.; Tanabe, Y. *J. Phys. Soc. Jpn.* **1958**, *13*, 880.
(27) (a) Macfarlane, R. M. *J. Chem. Phys.* **1967**, *47*, 2066. (b) Fairbank, W. M.; Klauminger, G. K. *Phys. Rev. B: Solid State* **1973**, *B7*, 500.

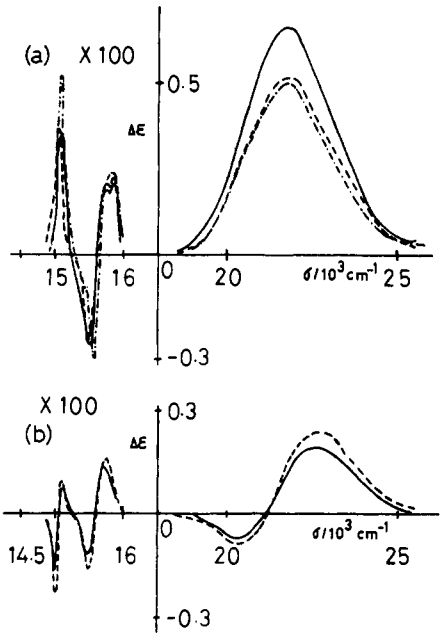

Figure 8. CD spectra of Λ-*cis*-$[Cr(NH_3)_2(en)_2]^{3+}$ (a) (-·-). Configurational (a) and vicinal (b) CD curves of *cis*-$[Cr(NH_3)_2(R\text{-diamine})_2]^{3+}$: *R*,*R*-chxn (—); *R*-pn (---).

is always negative, because it approximates to $-6B - 2C$, where B and C are the Racah electronic repulsion parameters. Thus, the energy ordering of the ^2E_g split components depends on the sign of the trigonal splitting parameter K. In the present case, K may be positive from the aforementioned assignment of the vicinal CD bands in the first-band region. Consequently, it can be expected that the $2\bar{A}$ component is located at a lower frequency side than the $\bar{E}$ one. Finally, the predicted CD pattern of the ^2E_g split components is negative and positive from the lower frequency side in the case of the vicinal effect due to the *R*-diamine ligands. This is the observed result as in Figures 1, 5, and 6, and Table IV. This energy ordering is the same as that from the magnetic circular dichroism study,[5] but it is reverse to that from the single-crystal absorption, CD, and circularly polarized luminescence studies.[6-8] The ^2E_g splitting interval is found to be 70–150 cm^{-1} by the present measurements, while it is determined to be 18 cm^{-1} by the single-crystal absorption and CD studies.[6,7] The cancellation between two opposite signed ^2E_g CD peaks may be responsible for the larger energy interval of the ^2E_g split components observed by the room-temperature solution CD measurements than by the low-temperature single-crystal ones.[6,7] It appears that the contribution of the *lel* conformation of the diamine ligands to the vicinal CD peaks in the spin-forbidden transitions does not differ from that of the *ob* conformation, though it is suggested that the conformational disorder in $2[Cr(en)_3]Cl_3 \cdot KCl \cdot 6H_2O$ crystals might result in the satellite bands around the $2\bar{A}$ and $\bar{E}$ components observed by the low-temperature single-crystal-polarized spectra.[6,7]

CD Spectra of the Tetraammine Complexes. The CD pattern of the tetraammine complexes in the first spin-allowed band region is quite similar to that of the vicinal CD curves due to the *R*-diamine ligands in the tris- and bis(diamine) complexes. As to the CD behavior in the spin-forbidden transitions, the two lowest frequency CD peaks are similar to the lowest frequency vicinal CD peaks due to the *R*-diamine ligands in the tris- and bis(diamine) complexes as in Figure 9; negative and positive CD peaks are observed from the lower frequency side. In the higher frequency $^2T_{1g} \leftarrow {}^4A_{2g}$ transition region, however, the signs of the CD peaks of the tetraammine (*R*-diamine) complexes are reverse to those of the vicinal CD peaks due to the *R*-diamine chelates in the bis(diamine) complexes as shown in Figure 9. This CD behavior may be elucidated by using the theoretical approaches for relating the energy ordering and the rotational strengths for the spin-forbidden transitions to those for the first spin-allowed transitions. By considering the holohedrized tetragonal (D_4)

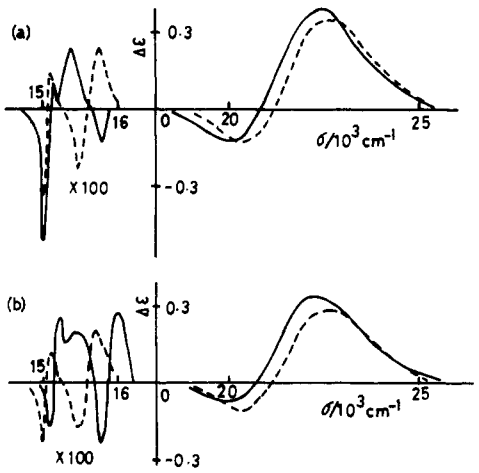

Figure 9. CD spectra of the tetraammine (diamine) complexes: (a) *R*,*R*-chxn (—); (b) *R*-pn (—). Vicinal CD curves of *cis*-diamminebis(diamine) complexes: (a) *R*,*R*-chxn (---); (b) *R*-pn (---).

symmetry for the present complexes, the angular-overlap model predicts that the $^4B_2(^4T_{2g})$ state is located at a lower frequency side than the $^4E(^4T_{2g})$ state for the tetraammine complexes and vice versa for the *cis*-diamminebis(diamine) complexes. The rotational strengths for the spin-forbidden transitions of tetragonal complexes may be given by those for the first spin-allowed transitions as follows:[2]

$$R(^2A_1(^2E_g)) = 24kR(^4E) \quad (6a)$$

$$R(^2B_1(^2E_g)) = 8k[R(^4E) + 4R(^4B_2)] \quad (6b)$$

$$R(^2E(^2T_{1g})) = 6k[R(^4E) + 2R(^4B_2)] \quad (6c)$$

$$R(^2A_2(^2T_{1g})) = 6kR(^4E) \quad (6d)$$

k is $\zeta^2/18[E(^4T_2) - E(^2\Gamma)]^2$, as given in eq 1a–c. From the above assignments of the tetragonal split components of the $^4T_{2g}$ state as well as eq 6c and d, it is predicted that the CD signs of the $^2T_{1g}$ split components are reverse to each other on the assumption of the same energy ordering for the $^2T_{1g}$ components for both the *cis*-diamminebis(diamine) and tetrammine complexes. This agrees with the observed CD pattern as in Figure 9. The same is true as far as the CD signs of the ^2E_g split components are concerned. From the following consideration, however, the energy ordering for these components of both the complexes is expected to reverse to each other. That is, this energy ordering depends on that for the tetragonal splitting of the first spin-allowed band as shown in the equation

$$\delta E = E(^2A_1) - E(^2B_1) = 192B^2[\delta\sigma/D_1^2 + \delta\pi/D_1D_2]$$

where D_1 and D_2 are the energy intervals between the doublet and quartet states and $\delta\sigma$ and $\delta\pi$ are McClure's parameters for the tetragonal ligand field splitting.[2,26] For amine ligands, $\delta\pi$ approximates zero. Then

$$\delta E = 96B^2[E(^4E) - E(^4B_2)]/(\Delta + 26B)^2 \quad (7)$$

where Δ is the ligand field parameter, $10Dq$, and $E(^4E) - E(^4B_2)$ is the tetragonal splitting of the $^4T_{2g}$ state. Accordingly, the energy ordering for the ^2E_g split components of the tetraammine complexes may be reverse to that of the *cis*-diamminebis(diamine) complexes, because the tetragonal splitting of each $^4T_{2g}$ state is reverse to one another. Therefore, the vicinal CD signs of the ^2E_g components are predicted to be negative and positive from the lower frequency side for the tetraammine (*R*-diamine) complexes and, in the case of the vicinal effect, due to the *R*-diamine ligands in the *cis*-diamminebis(diamine) complexes. This is the observed result as in Figure 9. The vicinal CD curves due to the *R*-diamine chelates in the present tetragonal complexes are assigned as in Table V.

Conclusions. We can make consistent assignments for the configurational and vicinal CD curves in the spin-forbidden and

the first spin-allowed transitions of the trigonal and tetragonal complexes of the type $Cr^{III}(N)_6$ in support of the theoretical approaches for the energy ordering and the rotational strengths. It is first demonstrated that room-temperature solution CD measurements can reveal the Kramers doublets of the ^2E_g state with a small spacing of less than 100 cm^{-1}. Within our present experimental and theoretical frameworks, the room-temperature solution CD peaks observed near 15 000 cm^{-1} are most likely attributed to the electronic origins of the spin-forbidden d-d transitions.

Acknowledgment. We thank Professor Yoichi Shimura of Osaka University for making the circular dichroism spectra available for the present work.

Contribution from the Christopher Ingold Laboratories, University College London, London WC1H OAJ, U.K.

Resonance Raman Spectroscopy of the Manganate(VI) Ion: Band Excitation Profiles and Excited-State Geometry

ROBIN J. H. CLARK,* TREVOR J. DINES, and J. MARK DOHERTY

Received October 26, 1984

The resonance Raman spectrum of the manganate(VI) ion $[MnO_4]^{2-}$, isomorphously doped into $K_2[CrO_4]$, has been studied over the range 406.7-676.4 nm. Detailed excitation profiles have been measured for the $\nu_1(a_1)$ and $2\nu_1$ bands throughout the region of the charge-transfer band of lowest energy. Theoretical analysis of these excitation profiles demonstrates that, on excitation from the ground (^2E) to resonant excited ($^2T_2$) states, the Mn-O bond length increases by 0.035 Å.

Introduction

In a number of recent papers[1-5] we have reported the results of detailed resonance Raman studies of some transition-metal tetraoxo and tetrathio anions. The molecules studied were all d^0 complexes, and in each case excitation was resonant with the lowest energy electric dipole allowed charge-transfer transition, $^1T_2 \leftarrow {}^1A_1$. From a theoretical model described by Clark and Stewart[1] the geometric changes attendant upon excitation to the $^1T_2$ state were calculated from computer simulations of the resonance Raman excitation profiles of the bands attributed to the $\nu_1(a_1)$ fundamental and its overtones.

Having established the value of resonance Raman spectroscopy as a probe of the electronic structure of such molecules,[6] it seemed appropriate to extend these studies to d^1 tetraoxo anions, of which the manganate(VI) ion, $[MnO_4]^{2-}$, may be regarded as the archetypal example. The molecular orbital scheme for $[MnO_4]^{2-}$ has been shown to be essentially the same as for $[MnO_4]^-$,[7,8] and the extra electron is contained within the lowest energy antibonding orbital, which has e symmetry, giving rise to a ^2E ground term (cf. $^1A_1$ for $[MnO_4]^-$). As for $[MnO_4]^-$, the charge-transfer band of lowest energy results from the promotion of an electron from the t_1 nonbonding orbitals (localized on the oxygen atoms) to the e antibonding orbitals. The excited configuration $(t_1)^5(e)^2$ gives rise to two $^2T_1$, two $^2T_2$, and one $^4T_2$ terms (cf. $^1T_1$, $^1T_2$, $^3T_1$, and $^3T_2$ for $[MnO_4]^-$). Thus, there are four fully allowed transitions for $[MnO_4]^{2-}$, producing four strong absorption bands, in place of the single one for $[MnO_4]^-$. The absorption spectrum of $[MnO_4]^{2-}$ in the 15 000-30 000-cm^{-1} region has been assigned on the basis of calculations that put the energies of the excited terms in the order $^2T_2 < {}^2T_2 \sim {}^2T_1 < {}^2T_2$.[8-10] There is also a weak band at around 12 000 cm^{-1} assigned to the $^2T_2 \leftarrow {}^2E$ ligand field transition resulting from the promotion of the electron in the e antibonding orbital to the (next lowest energy) t_2 antibonding orbital. The energy of the $^4T_2$ state has not been determined, but it is probably less than those of the other four states.

Table I. Band Wavenumbers of the $[MnO_4]^{2-}$ Ion Measured from Resonance Raman Spectra of $[MnO_4]^{2-}$ in $K_2[CrO_4]$ Recorded at ca. 15 K

assgnt	wavenumber/cm^{-1}	assgnt	wavenumber/cm^{-1}
$\nu_4(t_2)^a$	348 ± 1	$3\nu_1(A_1)$	2433.5 ± 0.5
$\nu_1(a_1)$	813.9 ± 0.5	$2\nu_1 + \nu_3(T_2)$	2452.6 ± 1.0
$\nu_3(t_2)$	832.3 ± 1.0	$4\nu_1(A_1)$	3235 ± 2
$2\nu_1(A_1)$	1625.5 ± 0.5	$3\nu_1 + \nu_3(T_2)$	3255 ± 2
$\nu_1 + \nu_3(T_2)$	1643.2 ± 0.5		

[a] Overlapped by the $\nu_2(e)$ band of the $[CrO_4]^{2-}$ ion.

There have been three previous resonance Raman studies of $[MnO_4]^{2-}$, all involving excitation within the region of the $^2T_2 \leftarrow {}^2E$ charge-transfer band of lowest energy. The results of these are summarized as follows: (1) a measurement of the excitation profiles of the ν_1 and $2\nu_1$ bands of $K_2[MnO_4]$ at room temperature;[11] (2) a study of the resonance Raman spectrum of $[MnO_4]^{2-}$ doped into CsI, recorded at 80 K, and a measurement of the excitation profile of the ν_1 band;[12] (3) wavenumber measurements of the resonance Raman bands of $K_2[MnO_4]$ and $Ba[MnO_4]$.[13]

The purpose of the present paper is to report, on the basis of dye laser excitation, the results of detailed measurements of the $\nu_1(a_1)$ and $2\nu_1$ Raman band excitation profiles. These measurements permit a more detailed analysis to be made of the charge-transfer band of lowest energy and permit an evaluation of the geometric change attendant upon excitation to the lowest $^2T_2$ state. Resonance Raman spectra were obtained from samples of $[MnO_4]^{2-}$ isomorphously doped into $K_2[CrO_4]$, for which extensive electronic absorption data have been reported by Day et al.[14]

Experimental Section

$K_2[MnO_4]$ was prepared by using the method of Nyholm and Woolliams.[15] Crystals of $[MnO_4]^{2-}$ doped into $K_2[CrO_4]$ were grown by slow

(1) Clark, R. J. H.; Cobbold, D. G.; Stewart, B. *Chem. Phys. Lett.* **1980**, *69*, 488. Clark, R. J. H.; Stewart, B. *J. Am. Chem. Soc.* **1981**, *103*, 6593.
(2) Clark, R. J. H.; Dines, T. J.; Wolf, M. L. *J. Chem. Soc., Faraday Trans. 2* **1982**, *78*, 679.
(3) Clark, R. J. H.; Dines, T. J. *J. Chem. Soc., Faraday Trans. 2* **1982**, *78*, 723.
(4) Clark, R. J. H.; Dines, T. J. *Inorg. Chem.* **1982**, *21*, 3585.
(5) Clark, R. J. H.; Dines, T. J.; Proud, G. P. *J. Chem. Soc., Dalton Trans.* **1983**, 2019.
(6) Clark, R. J. H. *ACS Symp. Ser.* **1983**, *No. 211*, 509.
(7) Ziegler, T.; Rauk, A.; Baerends, E. J. *Chem. Phys.* **1976**, *16*, 209.
(8) Jasinski, J. P.; Holt, S. L. *J. Chem. Soc., Faraday Trans. 2* **1976**, *72*, 1304.
(9) DiSipio, L.; Oleari, L.; Day, P. *J. Chem. Soc., Faraday Trans. 2* **1972**, *68*, 776.
(10) Vanquickenborne, L. G.; Verdonck, E. *Inorg. Chem.* **1976**, *15*, 454.
(11) Chao, R. S.; Khanna, R. K.; Lippincott, E. R. *J. Raman Spectrosc.* **1975**, *3*, 121.
(12) Martin, T. P.; Onari, S. *Phys. Rev. B: Solid State* **1977**, *15*, 1093.
(13) Jubert, A. H.; Varetti, E. L. *J. Mol. Struct.* **1982**, *79*, 285.
(14) Day, P.; DiSipio, L.; Ingletto, G.; Oleari, L., *J. Chem. Soc., Dalton Trans.* **1973**, 2595.
(15) Nyholm, R. S.; Woolliams, P. R. *Inorg. Synth.* **1968**, *11*, 57.

0020-1669/85/1324-2088$01.50/0